

Eswar Damaraju<sup>a,b,\*</sup>, Enzo Tagliazucchi<sup>c</sup>, Helmut Laufs<sup>d,e</sup>, Vince D Calhoun<sup>a,b</sup>

<sup>a</sup>*The Mind Research Network, Albuquerque, New Mexico, USA*

<sup>b</sup>*Department of Electrical and Computer Engineering, University of New Mexico, Albuquerque, USA*

<sup>c</sup>*Departamento de Física, Universidad de Buenos Aires, Buenos Aires, Argentina*

<sup>d</sup>*Department of Neurology and Brain Imaging Center, Goethe University Frankfurt am Main, Germany*

<sup>e</sup>*Department of Neurology, Christian Albrechts University, Kiel, Germany*

---

## Abstract

Interest in time-resolved connectivity in fMRI has grown rapidly in recent years. The most widely used technique for studying connectivity changes over time utilizes a sliding windows approach. There has been some debate about the utility of shorter versus longer windows, the use of fixed versus adaptive windows, as well as whether observed resting state dynamics during wakefulness may be predominantly due to changes in sleep state and subject head motion. In this work we use an independent component analysis (ICA)-based pipeline applied to concurrent EEG/fMRI data collected during wakefulness and various sleep stages and show: 1) connectivity states obtained from clustering sliding windowed correlations of resting state functional network time courses well classify the sleep states obtained from EEG data, 2) using shorter sliding windows instead of longer non-overlapping windows improves the ability to capture transition dynamics even at windows as short as 30 seconds, 3) motion appears to be mostly associated with one of the states rather than spread across all of them 4) a fixed tapered sliding window approach outperforms an adaptive dynamic conditional correlation approach, and 5) consistent with prior EEG/fMRI work, we identify evidence of multiple states within the wakeful condition which are able to be classified with high accuracy. Classification of wakeful only states suggest the presence of time-varying changes in connectivity in fMRI data beyond sleep state or motion. Results also inform about advantageous technical choices, and the identification of different clusters within wakefulness that are separable suggest further studies in this direction.

---

## 1. Introduction

The human brain continuously engages in mental activities that include introspection, theory of mind, and future planning, even when not actively pursuing a task. Fluctuations during the resting state have been shown to show functional network topology similar to that observed in task imaging studies (Calhoun et al., 2008; Smith et al., 2009). Since the first reports on time varying functional connectivity during task performance (Sakoğlu et al., 2010) and during a typical resting functional magnetic resonance imaging (fMRI) scan (Chang and Glover, 2010; Sakoğlu et al., 2010), there has been interest in studying and characterizing the changes in functional connectivity between brain regions on a shorter time scale, also referred to as time-resolved or dynamic functional connectivity (Calhoun et al., 2014; Hutchison et al., 2013). Recent years have seen a sharp increase in development of novel methods to characterize these dynamics (Allen et al., 2012a; Cribben et al., 2013; Kang et al., 2011; Tagliazucchi et al., 2012a; Vidaurre et al., 2017; Yaesoubi et al., 2015a) (see (Prete et al., 2017) for a thorough review).

One popular method to estimate connectivity dynamics in functional neuroimaging data is the use of sliding windows to estimate the connectivity between regions/networks. These time-varying connectivity estimates, when computed on the time courses from brain regions or seeds defined a

---

\*Corresponding author

Email address: [edamaraju@mrn.org](mailto:edamaraju@mrn.org) (Eswar Damaraju)

17 courses of networks obtained from blind decomposition techniques such as independent components  
18 analysis (ICA) are referred to as dynamic functional network connectivity (dFNC). In this work we  
19 focus on the latter, which leverages the benefits of ICA including data-driven identification of networks,  
20 robustness to noise, separation of overlapping signals of interest, and estimation of homogeneous  
21 networks that capture individual subject variability (Calhoun and de Lacy, 2017; Yu et al., 2017).  
22 Using an ICA based pipeline, Allen et al. (2012a) reported the presence of stable, recurring connectivity  
23 patterns/states obtained from clustering pairwise correlation estimates of windowed time courses of  
24 ICA derived intrinsic networks from resting fMRI data and more recently (Abrol et al., 2017) showed  
25 connectivity patterns and dynamic metrics are highly replicable across multiple independent data  
26 sets. However, a few studies have raised concerns over the quality of connectivity estimates obtained  
27 using the sliding window method (Lindquist et al., 2014; Smith et al., 2011), choice of window size  
28 (Hindriks et al., 2016; Leonardi and Van De Ville, 2015; Sakoğlu et al., 2010; Zalesky and Breakspear,  
29 2015), and the ability of the method to capture meaningful state transitions (Shakil et al., 2016).  
30 Others have primarily attributed the observable changes in connectivity in resting fMRI data to sleep  
31 state, sampling variability and head motion (Laumann et al., 2016).

32 In our prior concurrent EEG/fMRI work (Allen et al., 2017), windows corresponding to distinct  
33 dFNC connectivity states estimated using a sliding-window correlation method were associated with  
34 distinct electrophysiological signatures during both eyes open and eyes closed awake conditions and  
35 showed the ability of the method to track subject vigilance. However, since subjects were mostly  
36 awake throughout the scan sessions, simultaneously acquired electroencephalogram (EEG) data did  
37 not show enough state transitions from wakefulness to assess how well observed dFNC state transitions  
38 correspond to neurobiological state transitions i.e. observable changes in subject sleep state from  
39 EEG data.  
40

41 Here we use simultaneous EEG-resting fMRI data collected continuously over 50 minutes while  
42 the subjects transitioned between wakefulness and different sleep stages (defined by EEG-based sleep  
43 scoring) and assessed the ability of sliding window based dFNC measures to track the changes across  
44 these different wakefulness states. In addition to comparing the dFNC measure to sleep, this study  
45 provides us an opportunity to evaluate the impact of several technical choices within a real world  
46 dataset rather than in simulations (Leonardi and Van De Ville, 2015; Sakoğlu et al., 2010). For  
47 example, we compare the impact of the length of the sliding window on our ability to predict sleep  
48 stage. Windows should be short enough to be a good compromise between the ability to capture time  
49 varying connectivity without being too sensitive to noise. In addition, we compare a ‘fixed length’  
50 sliding window approach to a method from econometrics which has been applied to fMRI data, the  
51 dynamic conditional correlation (DCC) (Engle, 2002; Lindquist et al., 2014). DCC uses an adaptive  
52 window size and has been reported to show better test-rest reliability compared to ‘fixed length’  
53 sliding-window methods in estimating time varying functional connectivity (Choe et al., 2017). We  
54 also evaluate the relationship of the estimated states to motion, in particular we were interested in  
55 whether all states would show a similar relationship to motion or whether a subset of states captures  
56 the variance associated with motion.

## 57 2. Methods

### 58 2.1. Data acquisition

59 Resting state functional MRI data was collected from 55 subjects for 52 minutes each (1505  
60 volumes of echo planar images, repetition time (TR)=2.08 s, TE = 30 ms, matrix 64 x 64; FOV  
61 = 192 mm<sup>2</sup>, Thickness=2 mm, 1 mm gap between slices) on a Siemens 3T Trio scanner while the  
62 subjects rested with their eyes closed (details in (Tagliazucchi et al., 2012b)). Simultaneous EEG was  
63 acquired on 30 EEG channels with FCz as the reference (sampling rate = 5 kHz, low pass filter =  
64 250 Hz, high pass filter = 0.016 Hz) using an MR compatible device (BrainAmp MR+, BrainAmp  
65 ExG; Brain Products, Gilching, Germany).

EEG data underwent MRI and pulse artifact correction based on average artifact subtraction (Allen et al., 1998), followed by ICA-based residual artifact rejection. This data was subsequently sleep staged into wakeful (W), drowsy/light sleep (N1), moderate sleep (N2), and deep sleep (N3) stages by a sleep expert per American Academy of Sleep Medicine (AASM) criteria (AASM and Iber, 2007) resulting in a hypnogram for the scan duration for each subject. None of the participants went into REM sleep stage during the scan period. The first 5 volumes of functional imaging data were discarded to account for T1 equilibration effects. The data were then corrected for head movement (rigid body) and slice timing differences. Subject data was then spatially normalized to MNI template space using SPM12 toolbox and resampled to 3 mm<sup>3</sup> isotropic voxel resolution. Since the scan duration was long, we detrended each voxel time series using a high model order (21) polynomial. The subject brain voxel data were then spatially smoothed to 5 mm FWHM using AFNI's 3dBlurInMask. Finally, the voxel time courses were variance normalized (z-scored).

### 2.3. Independent component estimation

We performed a group independent component analysis (Calhoun et al., 2001; Calhoun and Adali, 2012) using the GIFT toolbox (<http://mialab.mrn.org/software/gift>) to decompose the data into 100 spatially independent components each associated with a coherent time course. First subject data were reduced in time to 1400 points using principal components analysis (PCA). These time reduced datasets were then concatenated in time and a group PCA was used to further reduce the data to 100 orthogonal directions of maximal variance. Spatial ICA analysis was performed on this data to obtain 100 spatially independent components using infomax algorithm. To ensure stability of decomposition, the Infomax ICA algorithm was repeated 20 times in ICASSO (Himberg et al., 2004) with random initialization, and aggregate spatial maps were estimated as the modes of the component clusters. Subject specific component maps and their associated time courses were obtained using spatio-temporal regression (Erhardt et al., 2011).

### 2.4. Component selection and dynamic FNC estimation

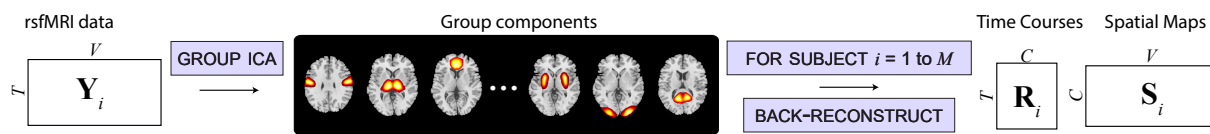
Of the 100 spatial ICA components, we identified 62 components as intrinsic connectivity networks (ICNs) in a semi-automatic manner using the spatial profile of component maps, and dominant low frequency spectral power of their time courses as described in (Allen et al., 2011). The corresponding ICN time courses of each subject were orthogonalized against estimated head movement parameters in a regression framework and then filtered using 5th order Butterworth filter with a passband of 0.01 to 0.15 Hz. Following (Allen et al., 2012a), we performed dynamic functional network connectivity analysis using the post processed ICN time courses. Briefly, we computed pairwise correlations between tapered windowed segments (a rectangular window of 30 TR (60s) convolved with a Gaussian kernel of  $\sigma = 3s$ ) of time courses sliding in steps of 1 TR. This resulted in 1500-30=1470 windows over which we estimated dFNC between 62 independent network time courses (1891 pairs). Since the number of samples are smaller than a static approach using all the timecourse information, we used a robust estimation strategy employing the graphical LASSO method (Friedman et al., 2008) by placing a penalty on the L1 norm of the precision matrix (inverse correlation matrix) to promote sparsity. Given the concerns with estimation of dFNC using shorter windows (Leonardi and Van De Ville, 2015; Lindquist et al., 2014; Smith et al., 2011), we repeated the analysis with longer tapered window sizes of size 45 TR, 60 TR, and shorter tapered window sizes of size 16 TR and 22 TR.

### 2.5. K-means clustering and comparison to EEG hypnogram

The dFNC windows from a given sliding window were clustered using the K-means algorithm in two steps consistent with our previous work (Allen et al., 2012a). We first computed a time course of standard deviation of dFNC matrices for each subject and selected subset of subject windows corresponding to local maxima in standard deviation as subject exemplars. These subset exemplars were clustered using K-means algorithm with Manhattan (L1) distance as distance measure. The

114 number of clusters was set to 5 based on the criterion of ratio of within to between cluster distance  
 115 of windows from cluster centroids, referred to as dFNC states. The obtained centroids were used  
 116 as starting points to cluster all the data. This two step procedure, one to identify initial starting  
 117 points and subsequent clustering of all window data using these starting points results in stable  
 118 centroid patterns across independent datasets. The K-means clustering (a hard clustering approach)  
 119 assigns each dFNC window to one of the dFNC states. This assignment of subject windows in time  
 120 to dFNC states results in a discrete vector referred to as state vector. Figure 1 shows the schematic  
 121 of the analysis pipeline used in the paper. We assessed the correspondence between subject dFNC  
 122 state vector and EEG-derived hypnogram using correlation. To further visualize the correspondence  
 123 between dFNC estimates from the sliding-window method and EEG-based subject hypnogram, we  
 124 project the multidimensional (1891) dFNC data into 2 dimensions using the t-distributed stochastic  
 125 neighborhood embedding (t-SNE) algorithm that preserves the distances between similar objects  
 126 in high dimensional space to low dimensions (van der Maaten et al., 2008). We also sought to  
 127 characterize the temporal properties of state vectors obtained from each modality by computing state  
 128 transition probabilities from these vectors and then compare the similarities between the two vectors.

### A IDENTIFICATION OF INTRINSIC CONNECTIVITY NETWORKS (ICNs)



### B DYNAMIC FUNCTIONAL NETWORK CONNECTIVITY (dFNC) ESTIMATION AND CLUSTERING

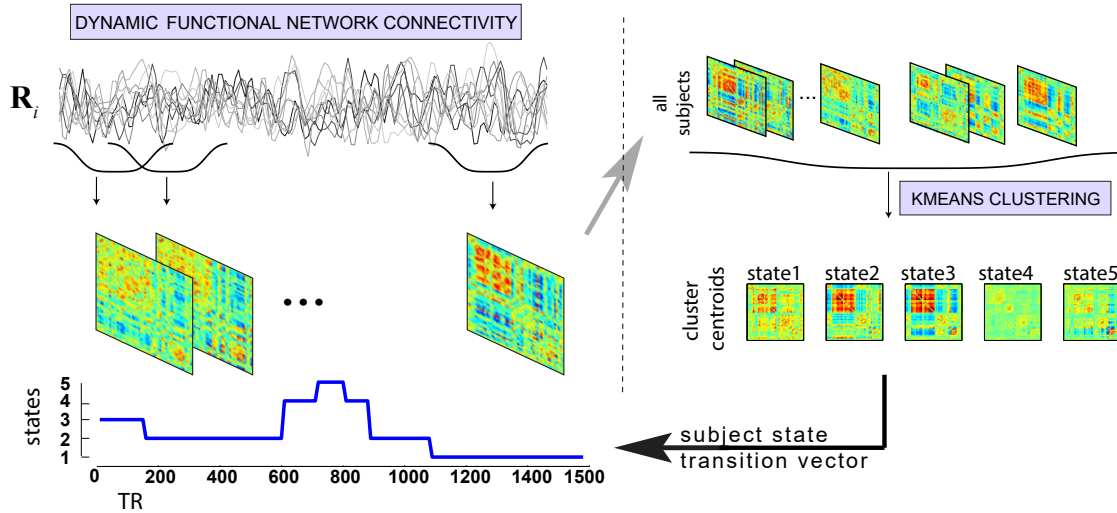


Figure 1: Schematic depicting resting fMRI data processing (adapted from (Damaraju et al., 2014)).

129 In our earlier work (Allen et al., 2017), we aligned FNC state vectors to EEG using the time  
 130 point corresponding to the center of the sliding window. As that study was performed during awake  
 131 conditions only (eyes open and eyes closed awake conditions), we did not have many EEG-based  
 132 transitions within the subject wakeful state. Since the data from this study has a ground truth  
 133 (EEG-based) hypnogram transition state vector informing of subject's sleep stage, we performed  
 134 a classification study using linear support vector machine (SVM) to see if the alignment of EEG  
 135 hypnogram best corresponds to start or middle or in-between shift (3, 5 or 7 TRs) of dFNC state vector  
 136 obtained from sliding window size of 30s. Prior to running SVM, the dFNC connectivity matrix (1891  
 137 pairs) was reduced to 30 dimensions using PCA. An 11 fold cross-validation was performed to assess  
 138 the consistency of best alignment. For each fold, 5 different subjects were left out and a linear SVM was  
 139 trained on remaining 50 subjects using libsvm package (<https://www.csie.ntu.edu.tw/~cjlin/libsvm/>).  
 140 A multi-class (all pairs/one-against-one) linear SVM model identifies support points in kernel space



141 that maximally separates each pair of classes (W-N1, W-N2, W-N3, N1-N2, N1-N3, N2-N3). Then each  
142 test case/window is assigned to the class that gets most votes. Both training and test balanced  
143 (averaged per class) accuracies were computed. The two awake dFNC states were collapsed into one  
144 for this analysis.

145 To identify optimal window size among the tested window sizes, we performed another linear  
146 SVM separately for dFNC windows obtained with each choice of window length. Similar cross-  
147 validation analysis as mentioned above was used. Finally, we also tested the performance of the  
148 DCC algorithm, which uses adaptive windowing, to track subject sleep state. The DCC algorithm  
149 fits univariate generalized autoregressive conditional heteroscedastic (GARCH) GARCH(1,1) models  
150 to each univariate time series to obtain standardized residuals and then applies an exponentially  
151 weighted moving average window on these standard residuals of each pair of time courses to compute  
152 a non-normalized version of time-varying correlation between the two time courses (see (Lindquist  
153 et al., 2014; Choe et al., 2017) for more details).

154 To investigate if wakeful state can be further clustered into meaningful sub-clusters as in our  
155 earlier work, we restricted our clustering analysis to the 26001 dFNC windows (State 1 for window  
156 size 30) that corresponded to the subject wakeful EEG condition. This analysis revealed 4 sub-clusters  
157 with distinct connectivity profiles. We ran a SVM classification analysis by holding out 6000 dFNC  
158 windows and performed a three fold cross validation on the remaining 20000 windows to estimate a  
159 model across a range of parameter C [0.1 to 10] for a linear kernel. The best model was then used to  
160 test the classification accuracy on the held out samples and we computed average per class accuracy  
161 and confusion matrix.

## 162 2.6. Head motion effects

163 To assess the impact of subject head motion on the connectivity estimates, we assessed the  
164 relationship between the subject head movement summaries and dFNC state vector. We computed  
165 framewise displacement (FD) and framewise data variation (DVARS) (Power et al., 2012) for each  
166 subject to represent their motion summary. We then computed the number of instances subject  
167 DVARS exceeds its mean by 2.5 times its standard deviation for each k-means state. A one-way  
168 ANOVA was then performed on the counts to see if certain states show significantly more motion  
169 related outliers. In addition, we plotted each subject state vector along with their FD and DVARS to  
170 visually assess if any of the states are contaminated by head movement.

## 171 3. Results

172 The sixty-two ICNs selected for subsequent analysis are depicted in Figure 2. These components  
173 are grouped into subcortical (5), auditory (2), sensorimotor (10), visual (11), a set of higher order  
174 associative areas involved in attentional and executive control as well as cognitive control (19), default-  
175 mode regions (10) and cerebellar (5) components based on anatomical proximity and functional  
176 connectivity as in our earlier studies (Allen et al., 2012a, 2011). The selected 62 ICN labels are  
177 summarized in Table 1.

### 178 3.1. dFNC clustering results

179 The centroids (k=5) obtained from k-means clustering of dynamic FNC window data of all subjects  
180 are shown in Figure 3A. The centroids were ordered according to their frequency of occurrence in time  
181 (from the most awake state to the deepest sleep state), with the exception of state 2 Figure 3B. These  
182 centroids show distinct connectivity patterns from state to state. Estimation of modularity of the  
183 centroid states using the Louvain community detection algorithm (Rubinov and Sporns, 2011) resulted  
184 in three modules for states 1,2 and 3, and four modules for states 4 and 5. Although subcortical and  
185 cerebellar ICs belong to the same module in all states, they segregate as an additional module for  
186 states 4 and 5. We computed mean within module connectivity strength and the top 12 ICs for each  
187 module are shown in Figure 3C.

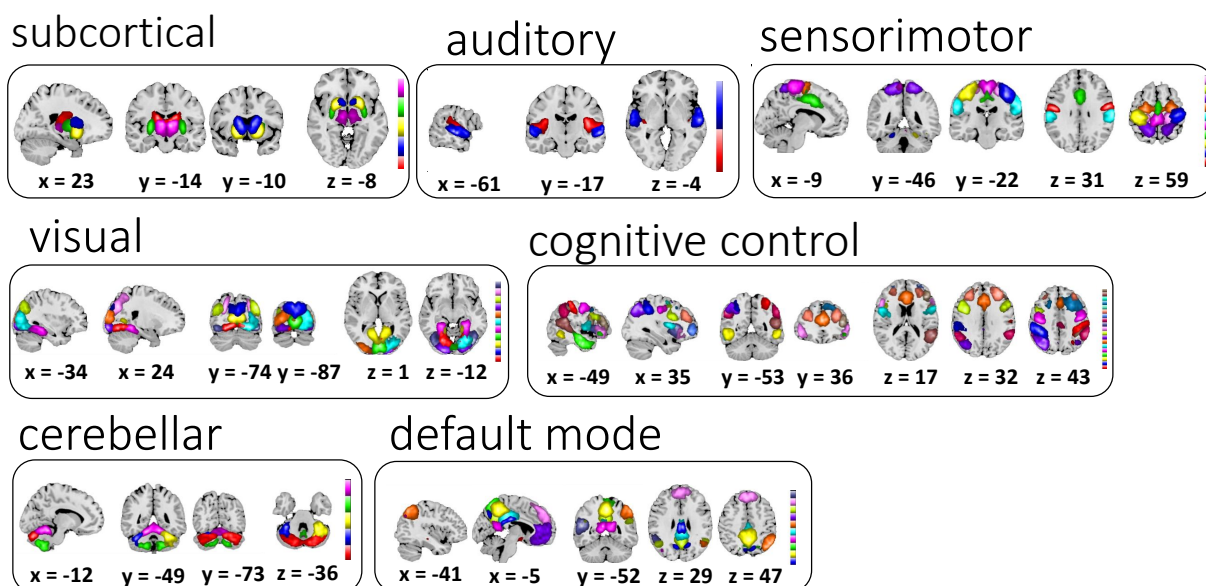


Figure 2: Sixty-two selected ICNs for further analysis were grouped into 7 modules using previously reported methods (Allen et al., 2012b).

### 188 3.2. Do clustered connectivity states correspond to sleep states?

189 The subject-state vectors are sorted by sleep state (W, N1, N2 and N3) and frequency counts by  
 190 sleep state were obtained and are shown in Figure 4. As seen in the figure, connectivity patterns  
 191 in states 1 and 2 predominantly occur in the awake state while the patterns seen in states 3, 4 and  
 192 5 occur more frequently as subjects fall into different sleep states gradually with the connectivity  
 193 pattern in state 5 occurring during N3 (deep) sleep stage.

194 We tested the correspondence between subject state vectors obtained through clustering dFNC  
 195 matrices and subject hypnograms obtained by computing the cross-correlation between the two vectors.  
 196 Figure 5 shows examples of subjects with the two best and the two worst correlations between the  
 197 two. As seen in the figure, the best subject showed a correlation of 0.89 between his/her hypnogram  
 198 and state vector. The subjects that showed the poorest correlation between the two primarily tended  
 199 to stay awake throughout the scan session, and the dFNC state vector showed transitions between  
 200 awake related states 1 and 2.

201 The results assessing the correspondence between subject dFNC state vector and his/her hypnogram  
 202 are summarized in Figure 6. For this projection, a random sample of 400 dFNC windows by state (total  
 203 2000 points) were visualized using the t-SNE algorithm and were color coded with their corresponding  
 204 k-means cluster assignment (Fig 6A) or by sleep stage obtained from the respective hypnogram (Fig  
 205 6B). Both awake states from the k-mean clustering are grouped together and show a transition from  
 206 wakefulness to deeper sleep stages that occurs gradually along a smooth trajectory. This result shows  
 207 that the dFNC estimates using the sliding window method and subsequent clustering correspond well  
 208 to neurophysiological states as estimated via the EEG-based hypnogram.

### 209 3.3. How does motion affect the clustering?

210 To assess the effect of subject head movement during the scan on dFNC clustering results, we  
 211 computed the number of windows with significant subject head movements (points greater than  
 212 2.5 standard deviations from mean framewise displacement) for each dFNC state and also visually  
 213 assessed subject dFNC state vector and mean framewise displacement vectors. State 2 is associated  
 214 with larger head movements during the scan relative to the other states. The number of significant

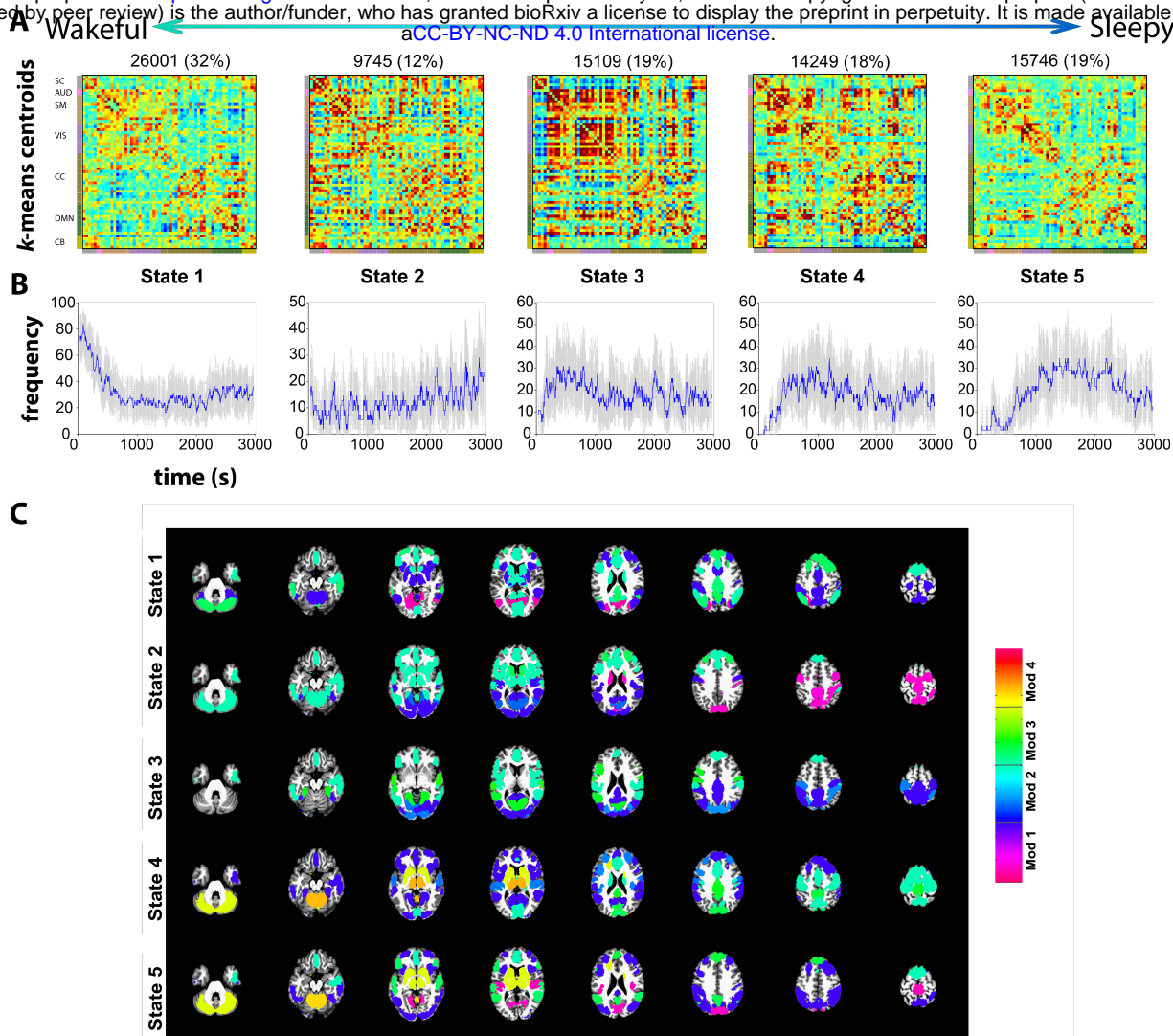


Figure 3: Cluster centroids from k-means clustering of dFNC window data for window size 30 (A) and the frequency of occurrence of each state in time (B). The standard errors for the frequency of occurrence were computed using 100 bootstrap resamples of the subject dFNC window data. (C) The modularity of the centroids is computed using the Louvain algorithm ("modularity\_louvain\_und\_sign.m" function in the Brain Connectivity toolbox) resulting in three modules (Mod) for states 1,2 and 3 and four modules for states 4 and 5. The top 12 ICs with highest mean within module FC are depicted scaled by mean within module FC. Note that the weights (mean within module connectivity) are lower in states 1 and 5 compared to states 2, 3 and 4.

215 head movements by state are shown in Supplemental Figure S1A. A couple of example subject state  
216 vectors and their head movement summary (FD) vectors are also shown in Supplemental Figure S1B.

### 217 3.4. Characterization of temporal dynamics

218 Comparison of the temporal properties of state vectors obtained from each modality is summarized  
219 in (Figure 7). The average dwell times and frequency of occurrence of each state are consistent  
220 for data from both modalities. The state transition matrices show good correspondence with more  
221 probable transitions from W->N1, N1->N2, N2->N3 and transitions to the W state from all sleep  
222 stages. This is in line with our knowledge of progression into various sleep stages. However, we  
223 observe a higher average number of transitions between states from the dFNC clustering derived state  
224 vectors compared to those computed using the EEG derived hypnogram.

### 225 3.5. Alignment of EEG derived hypnogram and windowed dFNC data

226 The SVM classification results for best alignment of EEG hypnogram and dFNC window position  
227 are presented in Figure 8. The results suggest that both start and middle TR of dFNC window

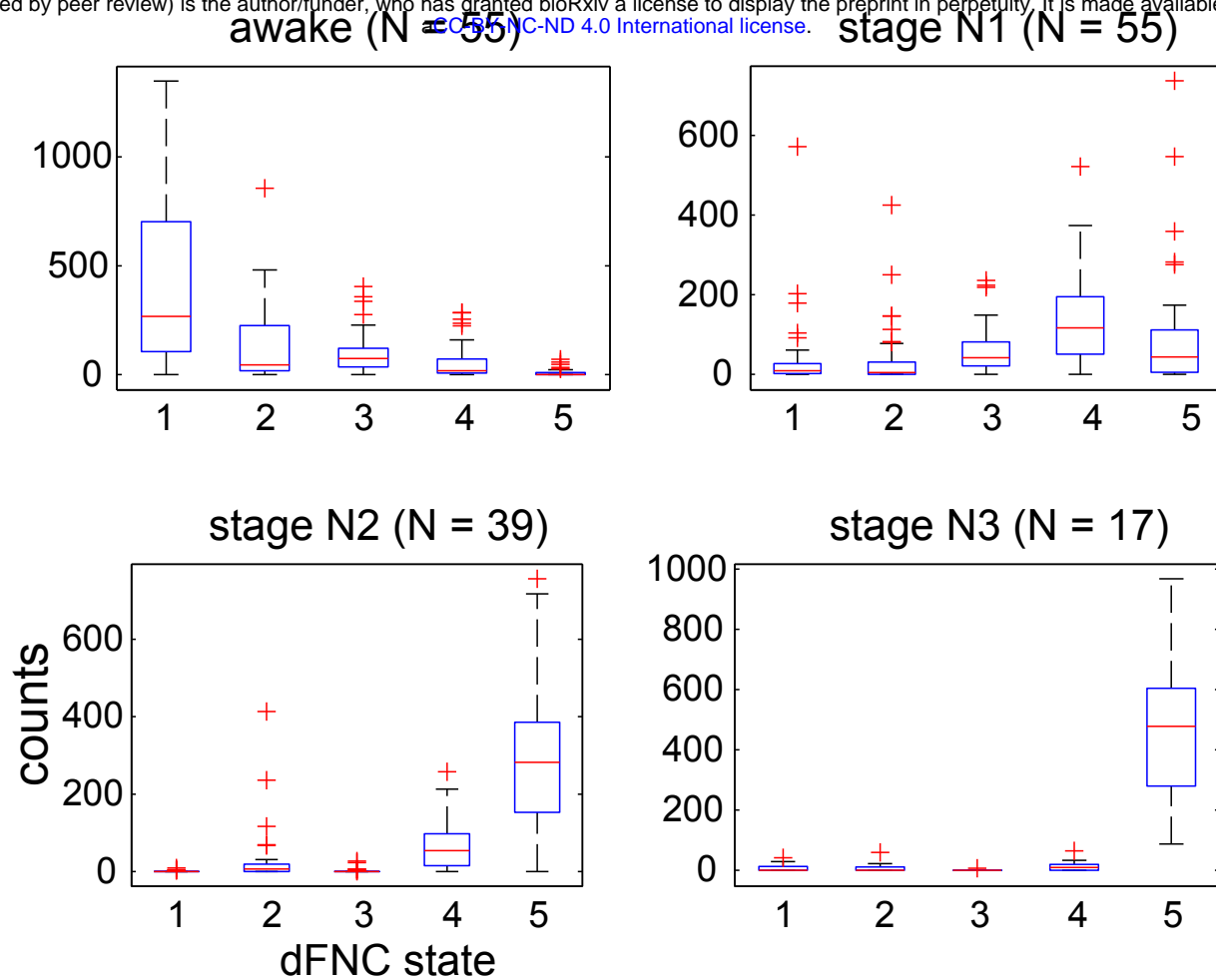


Figure 4: Frequency counts of state vector assignments obtained from k-means clustering of dFNC data sorted by hypnogram states. States 1 and 2 primarily occur during wakefulness, dFNC states 4 and 5 during N2 sleep stage and state 5 is predominant during deep sleep (N3 stage).

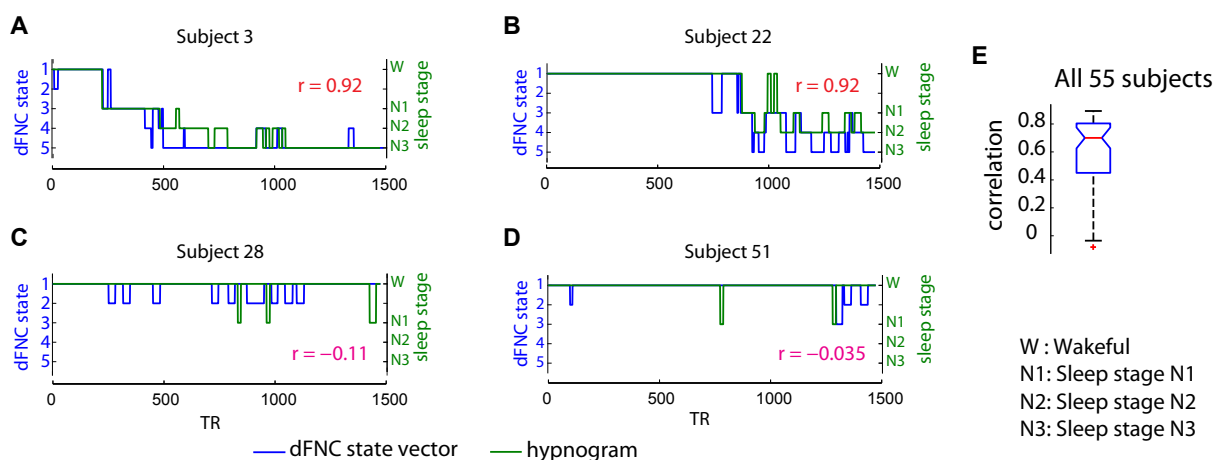


Figure 5: Comparison of subject state vectors obtained from k-means clustering of dFNC windows and EEG derived hypnograms for the two subjects with the highest correlation (A and B) and the two subjects with the lowest correlation (C and D). The overall distribution of the correlation between the two state vectors for all 55 subjects is presented in E. As seen, the subjects with low correlation tend to be awake throughout the scan session and the corresponding dFNC state vector transitions within the states 1 and 2 that are prevalent during wakefulness.

228 aligned to corresponding EEG hypnogram vector results in similar classification performance. However  
 229 in-between shifts resulted in poor classification accuracy.



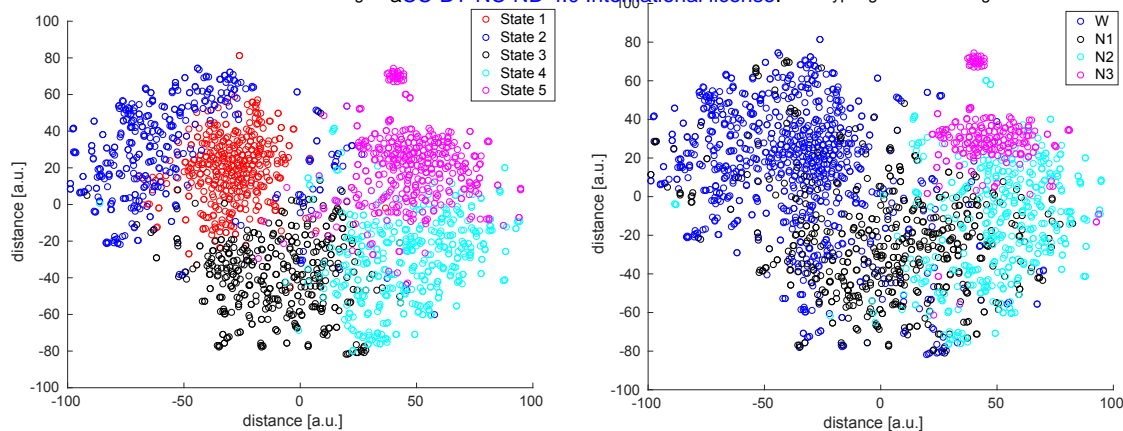


Figure 6: 2D Visualization of dFNC data: We selected 2000 random dFNC windows (400 per dFNC state) and projected the multidimensional (1891) data into 2 dimensions using the t-SNE algorithm. The resulting mapping was subsequently color coded by k-means clustering assignment into 5 states (A) and by the subject EEG hypnogram state of that point (B). The data dimension was reduced to 30 principal components and a perplexity value of 35 was used for this projection.

### 230 3.6. How well can we predict sleep stages from dFNC data?

231 The SVM classification accuracies comparing the prediction of subject hypnogram with dFNC  
232 estimates obtained using different window lengths is presented in Figure 9. As seen in the figure, the  
233 classification accuracy significantly increases with dFNC estimates from shorter to longer window  
234 sizes in training subject cases (the data SVM model has seen: one-way ANOVA  $F=342, p<1e-35$ ). The  
235 accuracies on left out test samples did not significantly differ with window sizes (one-way ANOVA  
236  $F=0.7, p>0.58$ ). These accuracy rates are consistent with earlier reports (Tagliazucchi et al., 2012b)  
237 however we show that these can be achieved using much shorter window lengths. The classification  
238 accuracies for dFNC estimates using DCC method performed poorly compared to those obtained  
239 using sliding window methods for all window sizes.

### 240 3.7. Does wakeful stage correspond to only one dFNC cluster?

241 Since our prior work (Allen et al., 2017) showed multiple wakeful states with distinct EEG spectral  
242 signatures, we further focused on the awake condition only to see if it can be reliably segmented  
243 into sub-clusters. A search for the optimal number of clusters using the elbow criterion yielded four  
244 clusters. The cluster centroids are depicted in Figure 10. Awake state cluster centroids 1 and 2  
245 resemble each other but differ in the strength of correlations in within and between module groupings.  
246 Awake state 4 resembles state 3 from the full dataset but distinguishes itself in anti-correlations  
247 between sensory (visual, motor and auditory) networks to higher order cognitive networks and also to  
248 the default-mode regions. Results from SVM classification of awake only cluster windows resulted in  
249 92% classification accuracy using a one-vs-rest linear SVM model with parameter  $C=1$ . The resulting  
250 confusion matrix is presented in Table 2. The classification accuracy reaches chance level of 25%  
251 when the class labels are permuted. This result suggests that the sub-clusters obtained from awake  
252 state are linearly separable with high accuracy.

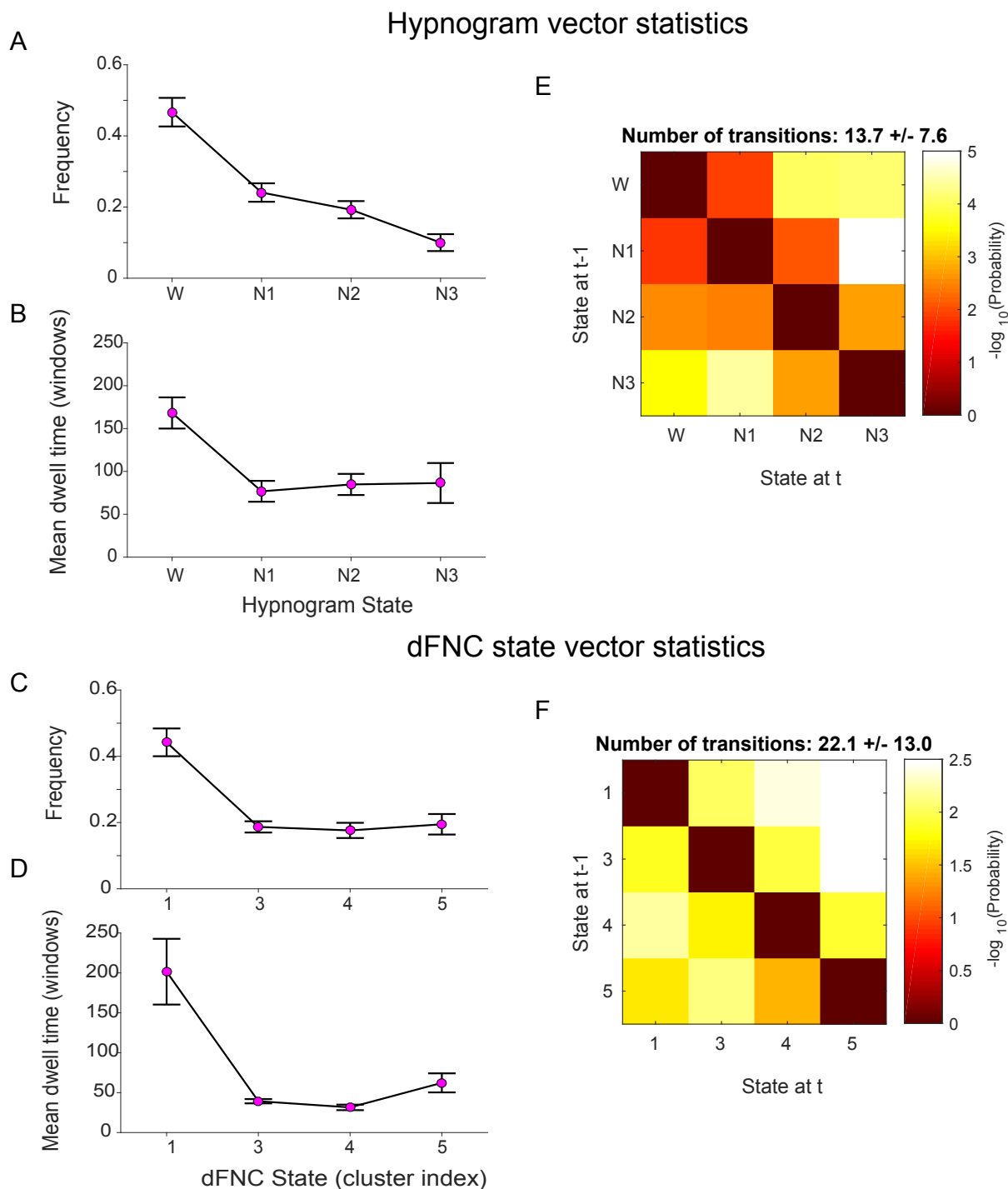


Figure 7: Comparison of state vector statistics and transition matrices computed from EEG-derived hypnograms and dFNC cluster derived subject state vectors. Hypnogram and dFNC state vector exhibit similar frequency of occurrences (A and C) and mean dwell times (B and D) respectively. The mean state transition matrices for hypnogram vectors (E) and dFNC state vectors (F) inform about the probability of transitioning from a given state  $i$  at time  $t-1$  to state  $j$  at time  $t$ . The probabilities are converted to  $-\log_{10}(\text{Probability})$  scale, so higher (yellow to white) intensity values mean lower probability to transition. For both modalities, these matrices demonstrate tendency to remain in a given state (diagonal values are lower). The transitions to neighboring states are more likely in both the hypnogram and the dFNC state vectors. While there is chance of transitioning from deep sleep N3 to any other state (W, N1 or N2), the probability of transitioning from wakefulness at time  $t-1$  immediately to deeper sleep stages (N2, N3) at time  $t$  is very low suggesting gradual transition from W to N3 stage. Note that dFNC states 1 and 2 are combined for this analysis.

<b>IC 58</b> (0.97)					R Middle Temporal Gyrus	331	53.568	-57	-58	-7	
R Caudate Nucleus	626	52.15	18	-16	20	R Middle Temporal Gyrus	151	37.405	60	-52	-7
<b>IC 27</b> (0.98)						<b>IC 84</b> (0.88)					
R Caudate Nucleus	786	66.366	12	14	8	R Inferior Temporal Gyrus	568	41.245	45	-13	-25
<b>IC 91</b> (0.76)						<b>IC 60</b> (0.95)					
L Putamen	342	87.587	-21	8	-7	L Postcentral Gyrus	272	49.711	-48	-13	47
R Putamen	338	92.203	24	11	-7	R Precentral Gyrus	260	43.566	45	-10	41
<b>IC 98</b> (0.68)						<b>IC 63</b> (0.96)					
R Putamen	372	94.022	27	-1	2	L Insula Lobe	324	44.285	-36	2	11
L Putamen	359	113.49	-27	-4	2	R Insula Lobe	264	52.788	36	5	11
<b>IC 20</b> (0.98)						<b>IC 74</b> (0.93)					
R Thalamus	861	87.008	6	-13	5	L Anterior Cingulate Cortex	668	51.736	-3	26	26
						<b>IC 47</b> (0.97)					
<b>Auditory Networks</b>	$V_{\ell}$	$t_{\max}$	Coordinate			L Angular Gyrus	583	48.228	-42	-70	41
						<b>IC 65</b> (0.94)					
<b>IC 34</b> (0.98)						L Inferior Frontal Gyrus (p. Opercularis)	396	42.552	-42	11	29
R Insula Lobe	438	48.445	33	-25	17	R Inferior Frontal Gyrus (p. Opercularis)	96	29.433	42	14	32
L Rolandic Operculum	415	42.729	-45	-22	11	<b>IC 89</b> (0.92)					
<b>IC 14</b> (0.98)						L Inferior Frontal Gyrus (p. Opercularis)	465	40.334	-54	14	8
R Superior Temporal Gyrus	347	46.328	60	-16	-4	R Inferior Frontal Gyrus (p. Triangularis)	213	35.37	54	26	5
L Superior Temporal Gyrus	303	35.198	-60	-13	2	<b>IC 53</b> (0.96)					
						R Insula Lobe	421	50.671	36	20	-1
<b>Sensorimotor Networks</b>	$V_{\ell}$	$t_{\max}$	Coordinate			L Insula Lobe	305	47.124	-33	17	8
						<b>IC 33</b> (0.98)					
<b>IC 2</b> (0.98)						R SupraMarginal Gyrus	286	44.455	57	-46	35
L Postcentral Gyrus	229	52.196	-48	-10	32	L Inferior Parietal Lobule	278	44.221	-54	-49	38
R Postcentral Gyrus	221	53.635	57	-4	29	<b>IC 32</b> (0.98)					
<b>IC 4</b> (0.98)						R Superior Orbital Gyrus	288	37.454	27	56	-1
R Precentral Gyrus	570	71.156	36	-22	53	L Middle Frontal Gyrus	274	33.346	-30	53	2
<b>IC 7</b> (0.98)						<b>IC 51</b> (0.97)					
L Postcentral Gyrus	595	65.889	-36	-25	56	R Middle Frontal Gyrus	397	43.207	30	44	29
<b>IC 81</b> (0.9)						L Middle Frontal Gyrus	280	34.033	-33	38	29
R Middle Cingulate Cortex	815	52.287	3	-7	47	<b>IC 49</b> (0.98)					
<b>IC 3</b> (0.98)						R Inferior Temporal Gyrus	328	40.668	63	-31	-19
R Paracentral Lobule	728	57.783	3	-28	68	L Middle Temporal Gyrus	259	38.391	-63	-43	-13
<b>IC 55</b> (0.97)						<b>IC 86</b> (0.86)					
R Postcentral Gyrus	416	46.245	54	-19	35	R Middle Frontal Gyrus	715	49.803	27	17	53
L Postcentral Gyrus	292	39.467	-60	-22	29	L Middle Frontal Gyrus	166	33.725	-27	23	53
<b>IC 80</b> (0.95)						<b>IC 78</b> (0.95)					
L Superior Frontal Gyrus	855	42.788	-21	-4	65	L SMA	673	57.132	-3	11	62
<b>IC 67</b> (0.96)						<b>IC 36</b> (0.98)					
L Superior Parietal Lobule	431	48.987	-21	-49	68	R Superior Temporal Gyrus	547	44.804	57	-49	20
R Superior Parietal Lobule	332	45.144	15	-49	65	<b>IC 96</b> (0.69)					
<b>IC 26</b> (0.98)						R Inferior Frontal Gyrus (p. Triangularis)	199	39.597	42	35	17
R Middle Temporal Gyrus	267	50.626	51	-67	2	R Inferior Frontal Gyrus (p. Opercularis)	110	30.408	51	11	23
L Middle Occipital Gyrus	171	39.173	-45	-70	5						
<b>IC 48</b> (0.98)						<b>Default-mode Networks</b>	$V_{\ell}$	$t_{\max}$	Coordinate		
R Precentral Gyrus	334	52.234	21	-22	59	<b>IC 18</b> (0.98)					
L Precentral Gyrus	150	45.439	-21	-25	59	R Middle Cingulate Cortex	134	45.344	3	-22	29
						R Precuneus	93	41.094	12	-64	35
<b>Visual Networks</b>	$V_{\ell}$	$t_{\max}$	Coordinate			<b>IC 75</b> (0.95)					
						R Precuneus	738	59.873	3	-52	50
<b>IC 77</b> (0.92)						<b>IC 83</b> (0.89)					
L Lingual Gyrus	719	52.696	-18	-73	-10	L Precuneus	687	52.332	0	-64	59
<b>IC 17</b> (0.98)						<b>IC 13</b> (0.98)					
L Cuneus	932	63.044	-3	-85	38	L Precuneus	532	60.221	-6	-52	14
<b>IC 11</b> (0.98)						<b>IC 59</b> (0.97)					
R Calcarine Gyrus	1133	61.631	15	-67	8	L Middle Cingulate Cortex	735	59.744	-3	-31	35
<b>IC 25</b> (0.98)						<b>IC 61</b> (0.95)					
L Calcarine Gyrus	752	64.739	3	-85	2	R Inferior Parietal Lobule	539	50.287	45	-58	50
<b>IC 38</b> (0.97)						<b>IC 57</b> (0.96)					
R Fusiform Gyrus	320	52.29	30	-49	-10	L Mid Orbital Gyrus	851	44.422	0	50	-13
L ParaHippocampal Gyrus	226	48.254	-27	-43	-10	<b>IC 24</b> (0.98)					
<b>IC 97</b> (0.73)						L Precuneus	443	81.554	0	-61	32
R Lingual Gyrus	972	43.732	18	-73	-7	<b>IC 35</b> (0.97)					
<b>IC 66</b> (0.95)						L Superior Medial Gyrus	885	43.348	-3	47	35
L Cuneus	939	46.324	-6	-97	14	<b>IC 29</b> (0.98)					
<b>IC 22</b> (0.98)						L Middle Temporal Gyrus	591	41.693	-51	-52	14
R Lingual Gyrus	674	51.127	21	-94	-7						
<b>IC 69</b> (0.94)						<b>Cerebellar Networks</b>	$V_{\ell}$	$t_{\max}$	Coordinate		
R Middle Occipital Gyrus	384	53.579	42	-73	35	<b>IC 16</b> (0.98)					
L Middle Occipital Gyrus	218	37.83	-39	-76	32	R Cerebellum (Crus 1)	1198	50.811	18	-76	-28
<b>IC 73</b> (0.94)						<b>IC 100</b> (0.61)					
L Superior Occipital Gyrus	375	44.761	-24	-73	35	L Cerebellum (Crus 1)	201	30.986	-36	-46	-34
R Middle Occipital Gyrus	191	42.562	33	-73	23	<b>IC 45</b> (0.97)					
<b>IC 50</b> (0.97)						R Cerebellum (VI)	568	42.816	30	-49	-34
R Inferior Occipital Gyrus	349	40.302	45	-73	-10	<b>IC 8</b> (0.98)					
L Lingual Gyrus	264	36.962	-33	-85	-16	R Cerebellum (IX)	837	48.11	15	-58	-49
						<b>IC 9</b> (0.98)					
<b>Cognitive Control Networks</b>	$V_{\ell}$	$t_{\max}$	Coordinate			R Cerebellum (IV-V)	987	62.466	12	-49	-19
<b>IC 76</b> (0.91)											
R Inferior Parietal Lobule	602	52.132	39	-40	50						
<b>IC 71</b> (0.95)											
L Inferior Parietal Lobule	552	53.538	-45	-37	44						

Table 1: **Peak activations of ICN SMs.** The quality index ( $I_q$ ) associated with each ICN is listed in parentheses adjacent to the component number;  $V_{\ell}$  = number of voxels in each cluster;  $t_{\max}$  = maximum  $t$ -statistic in each cluster; Coordinate = coordinate (in mm) of  $t_{\max}$  in MNI space, following LPI convention.

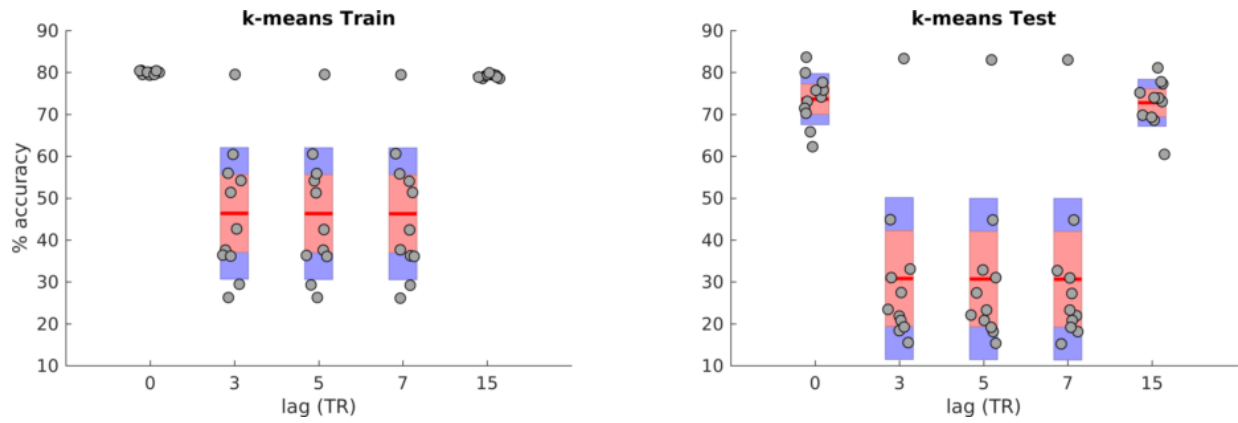


Figure 8: SVM classification accuracies for training (A) and test (B) cases of alignment between EEG hypnogram and subject dFNC state vector obtained using a window size of 30 TRs. The alignment is tested for lags 0, 3, 5, 7 and 15 TRs. Each point in the distribution corresponds to the balanced per class accuracy from one of the 11 cross-validation iterations of training data (left) that included data from 50 random subjects and the accuracy from left of test data (right) that included data from 5 remaining subjects.

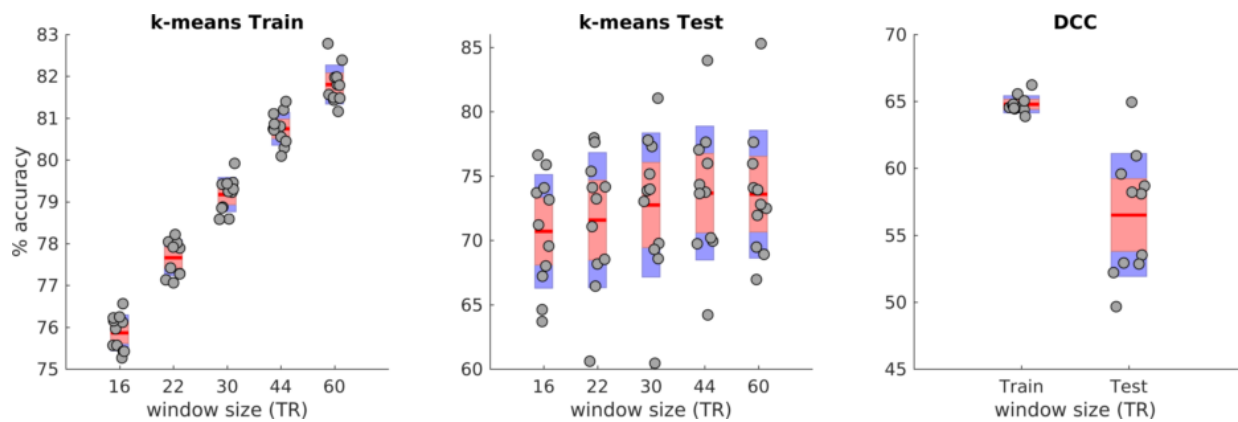


Figure 9: Linear SVM classification accuracies of subject sleep stage from dFNC estimates obtained using different window sizes for training (left), test (middle) data from 11 cross-validation iterations and the classification accuracies obtained from the DCC estimates for the same cross-validation scheme for training and left out test data are presented in the right.

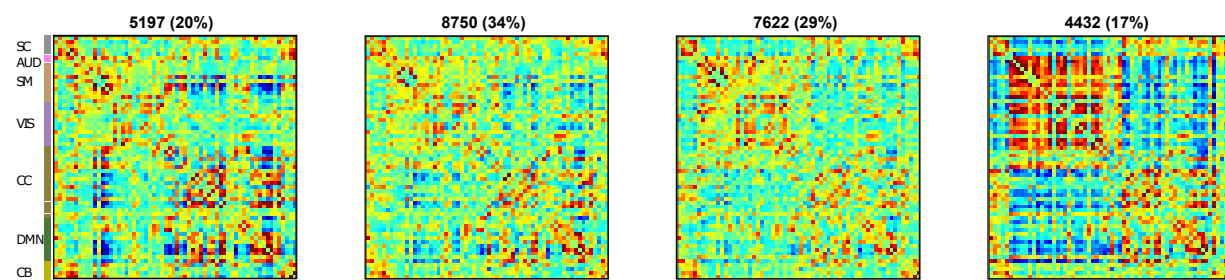


Figure 10: Cluster centroids from k-means clustering of window dFNC data of awake only state (State 1). The estimated clusters were observed to have meaningful and distinct structure.



		Predicted			
		AwState 1	AwState 2	AwState 3	AwState 4
Actual	AwState 1	91.8	4.2	3.4	0.6
	AwState 2	0.6	94.8	3.4	1.2
	AwState 3	1.9	5.5	89.7	2.7
	AwState 4	0.9	2.8	3.8	92.4

Table 2: **Awake state SVM classification confusion matrix.** The percent classification accuracy from linear SVM model for each of the four awake only K-means states. The high accuracy strongly suggests that these clusters are unlikely to be noise.

## 4. Discussion

In this work, using an ICA based pipeline, we assess the ability of sliding window correlation based dynamic functional network connectivity measures to capture neurophysiological state transitions obtained from sleep staging of EEG data that was concurrently acquired during resting fMRI acquisition. Results show a good correspondence between the subject state vectors obtained from k-means clustering of dFNC windows and subject hypnograms. We further demonstrate that distinct resting functional connectivity patterns are associated with wakeful and sleep states with dFNC state 1 predominantly occurring while subjects are awake, dFNC state 3 corresponding to reduced subject vigilance and early sleep stage (N1) and dFNC states 4 and 5 are more likely to be associated with deeper sleep stages. Deep sleep (N3) is primarily associated with dFNC state 5 across all subjects. One state (dFNC state 2) primarily captures variance associated with subject movement.

### 4.1. dFNC clustering estimates can reliably predict subject sleep state

Recently, using the same data reported in this work, [Haimovici et al. \(2017\)](#) showed good correspondence between centroids of windowed resting fMRI correlation data obtained from k-means clustering and those informed by an EEG-based hypnogram. In [Haimovici et al. \(2017\)](#), the connectivity measures were estimated from non-overlapping windows of length 100 seconds within fixed regions of interest and so precludes time varying connectivity information. Our work replicated the aforementioned result in [Haimovici et al. \(2017\)](#) despite several differences including the use of time-varying connectivity estimates from ICA derived network time courses as well as the use of overlapping windows with a step size of 1 TR. Using this approach, we show that high classification accuracies can be obtained for windows as short as 30 seconds (15 TRs).

Our results also demonstrated that dFNC estimates from sliding window correlation show higher accuracy compared to an adaptive windowless dynamic conditional correlation method. However, DCC estimates from sliding window based covariance estimates resulted in classification accuracies similar to those obtained from the sliding window method suggesting this parametric model of conditional correlation for resting fMRI data might be more sensitive to noise than smoother sliding window estimates when instantaneous conditional correlation estimates are computed.

Our analysis demonstrates that even window lengths as short as 30 seconds result in reasonable estimates of time-varying connectivity profiles with estimated dFNC clustering states showing good classification accuracy with subject hypnogram. This is in line with previous reports ([Shirer et al., 2012](#)) and suggests that the  $1/f_{min}$  recommendation for window length as recommended by [Leonardi and Van De Ville \(2015\)](#) might be too conservative ([Vergara and Calhoun, 2018](#)). In our case  $1/f_{min}$  would result in 100 sec (since  $f_{min} = 0.01$  Hz after filtering) and may limit our ability to capture dynamics for  $1/f$  spectral distributed BOLD data ([Zalesky and Breakspear, 2015](#)).

The observed differences between the individual dFNC state vector and the hypnogram can arise for the following reasons. The hypnogram is scored from EEG data epochs of 30 seconds and assigns each 30 second segment to a single hypnogram stage (W/N1/N2 or N3). The dFNC at a given instant is estimated from a window length 'w' on either side of the time point (past and future). However, k-means is a hard clustering approach and, as seen in Figure 6, there is ambiguity in the assignment of the data point with its immediate neighboring state (for example dFNC states 4 and 5 and corresponding N2 and N3 sleep stages) compared to the ground truth (hypnogram). Fuzzy k-means approaches can help mitigate this issue by allowing for states to overlap with one another ([Miller et al., 2016](#)). Another source of possible differences may be due to the different impact of noise (e.g. motion, MRI gradients) on the two signals which can hinder our ability of accurately estimating subject states.

### 4.2. Head motion appears to be separable from dynamic connectivity measures

Our dFNC clustering analysis reveals that motion appears to be mostly associated with one of the states (dFNC state 2) rather than spread across all of them. An examination of classification

301 least errors (about 10%) and N1 sleep stage had the most errors (approximately 40%), with deeper  
302 sleep stages having an error rate of about 20%. Further evaluation to determine if dFNC windows  
303 overlapping with larger head movements during the scan drive these errors suggested that motion only  
304 contributed to about 15% of misclassified cases evenly across wakeful and sleep stages i.e 15% of 10,  
305 40, 20 and 20 error rates of W, N1, N2, and N3 stages respectively. This suggests that dFNC windows  
306 exhibit larger variability during the N1 sleep stage compared to other sleep stages as observed in  
307 Supplemental Figure S2 leading to misclassification. This highlights the need to further identify  
308 additional sub-clusters in the N1 sleep stage and investigate if a fine grained EEG classification of  
309 this stage as proposed by Hori and colleagues (Hori et al., 1994) and recently demonstrated using  
310 EEG data (Jagannathan et al., 2018) can provide additional insights into large scale connectivity  
311 changes during the transition to sleep (Goupil and Bekinschtein, 2012).  
312

#### 313 4.3. Evidence of multiple dFNC sub-clusters states during wakefulness

314 The elbow criterion, computed as a ratio of between-cluster to within-cluster distance, was used to  
315 obtain an optimal k for clustering of the data using the k-means algorithm. Results suggest a 5 cluster  
316 solution within which we observe fewer (two) states from the wakeful portions of the scans than those  
317 reported earlier for data collected during the wakeful condition only (Allen et al., 2012b, 2017). This  
318 could be due to the fact that variability in dFNC fluctuations during wakefulness is lower compared  
319 to variability across different sleep stages (see Supplemental Figure S2). To evaluate this further, we  
320 performed a separate elbow criterion search and clustering of dFNC windows within only the wakeful  
321 state to see if additional clusters of meaningful time-varying connectivity profiles within and across  
322 subjects can be reliably estimated. Separate K-means clustering of dFNC windows from the awake  
323 only state (state 1) revealed additional sub-clusters not seen from clustering the data including all  
324 sleep stages. Windows corresponding to these sub-clusters are linearly separable with good accuracy  
325 using a linear SVM classifier. This result is in line with and extends recent reports showing replicable  
326 dFNC states in multiple independent datasets (Abrol et al., 2017) during (unconfirmed) wakeful  
327 conditions.

328 Some recent studies have argued that the observed connectivity states during wakefulness are  
329 primarily a reflection of sampling variability, changes in subject vigilance and partly reflect changes due  
330 to head movement (Laumann et al., 2016; Liegeois et al., 2017; Haimovici et al., 2017). Spontaneous  
331 eye blinks during wakefulness have also been shown to cause connectivity fluctuations in resting  
332 fMRI data (Wang et al., 2016). Another view is that time-varying connectivity changes in resting  
333 state fMRI can be modeled as hierarchical transitions between connectivity states consisting of two  
334 metastates: one corresponding to states with increased connectivity in brain regions involved in higher  
335 cognition and other corresponding to states with greater integration within sensory regions (Vidaurre  
336 et al., 2017). Another recent study identified strong correlation between dFC obtained using sliding  
337 window correlation of BOLD data and temporal dynamics of calcium signal during rest in mice brain  
338 recordings suggesting a neuronal origin of the observed dynamics (Matsui et al., 2018). In this work,  
339 we show distinct connectivity states during wakefulness that are separable via a cross-validated linear  
340 classifier. Future studies should evaluate the underlying neurobiological signatures of both sleep and  
341 wakefulness in greater detail.

#### 342 4.4. Limitations and future work

343 We did not compare the sliding window correlation method to alternative methods of dynamic  
344 connectivity methods like multiplication of temporal derivatives (Shine et al., 2015) and time-frequency  
345 approaches (Yaesoubi et al., 2015b). For classification analysis, we used linear SVM with cross-  
346 validation. The classification accuracies might improve with a non-linear (RBF or polynomial) kernel  
347 with additional optimization of the kernel parameter search space. Also, we reduced the functional  
348 connectivity matrix dimension using PCA before training the SVM model. Alternative feature  
349 selection models like recursive feature elimination might improve classification accuracy. However we

350 expect that the observed differences in accuracy of classification from dFNC data for different window  
351 lengths would remain even after employing more complex procedures. Also, in this work we show  
352 the presence of linearly separable (predictable) connectivity states during wakeful rest to extend our  
353 previous work and address some current technical controversies in the field. Going forward, it would  
354 be interesting to perform a hierarchical analysis of various sleep stages to evaluate the possibility  
355 of different states existing during different sleep stages as well as to further study the underlying  
356 neurobiological correlates of these states with the use of multimodal imaging data along with novel  
357 modeling techniques.

#### 358 *4.5. Conclusions*

359 In this work, using an ICA-based pipeline applied to concurrent EEG/fMRI data collected during  
360 wakefulness and various sleep stages we demonstrate that time varying connectivity estimates from  
361 sliding windowed correlations of resting state functional network time courses well classify the sleep  
362 states obtained from EEG data even for windows as short as 30 seconds. We show that head motion  
363 is mostly associated with one of the states rather than spread across all of them. Consistent with  
364 earlier work, we find increased variability in connectivity as subjects transition from wakefulness to  
365 sleep. We report linearly separable clusters within the wakeful state and suggest future directions for  
366 assessing their neurobiological relevance via hierarchical analysis of predictable states in various sleep  
367 stages measured with EEG-fMRI data including eye tracking during the wakeful condition.

#### 368 *4.6. Acknowledgements*

369 This work was funded by NIH P20GM103472, Ro1EB006841 and NSF EPSCoR 1539067 and  
370 the Bundesministerium für Bildung und Forschung (grant 01 EV 0703) and the LOEWE Neuronale  
371 Koordination Forschungsschwerpunkt Frankfurt (NeFF).

## 372 **Bibliography**

- 373 AASM, Iber, C., 2007. The AASM Manual for the Scoring of Sleep and Associated Events: Rules,  
374 Terminology and Technical Specifications. American Academy of Sleep Medicine.
- 375 Abrol, A., Damaraju, E., Miller, R. L., Stephen, J. M., Claus, E. D., Mayer, A. R., Calhoun,  
376 V. D., 2017. Replicability of time-varying connectivity patterns in large resting state fMRI samples.  
377 *Neuroimage* 163, 160–176.
- 378 Allen, E. A., Damaraju, E., Eichele, T., Wu, L., Calhoun, V. D., 2017. EEG Signatures of Dynamic  
379 Functional Network Connectivity States. *Brain Topography*, 1–16.
- 380 Allen, E. A., Damaraju, E., Plis, S. M., Erhardt, E. B., Eichele, T., Calhoun, V. D., 2012a. Tracking  
381 Whole-Brain Connectivity Dynamics in the Resting State. *Cerebral Cortex*.  
382 URL [http://cercor.oxfordjournals.org/content/early/2012/11/09/cercor.bhs352.](http://cercor.oxfordjournals.org/content/early/2012/11/09/cercor.bhs352.abstract)  
383 [abstract](http://cercor.oxfordjournals.org/content/early/2012/11/09/cercor.bhs352.abstract)
- 384 Allen, E. A., Erhardt, E. B., Damaraju, E., Gruner, W., Segall, J. M., Silva, R. F., Havlicek, M.,  
385 Rachakonda, S., Fries, J., Kalyanam, R., Michael, A. M., Caprihan, A., a. Turner, J., Eichele, T.,  
386 Adelsheim, S., Bryan, A. D., Bustillo, J., Clark, V. P., Feldstein Ewing, S. W., Filbey, F., Ford,  
387 C. C., Hutchison, K., Jung, R. E., a. Kiehl, K., Kodituwakku, P., Komesu, Y. M., Mayer, A. R.,  
388 Pearlson, G. D., Phillips, J. P., Sadek, J. R., Stevens, M., Teuscher, U., Thoma, R. J., Calhoun,  
389 V. D., 2011. A Baseline for the Multivariate Comparison of Resting-State Networks. *Frontiers in*



- 390 URL <http://www.pubmedcentral.nih.gov/articlerender.fcgi?artid=3051178&tool=pmcentrez&rendertype=abstract>
- 391
- 392
- 393 Allen, E. A., Erhardt, E. B., Wei, Y., Eichele, T., Calhoun, V. D., 2012b. Capturing Inter-Subject  
394 Variability With Group Independent Component Analysis of fMRI Data: a Simulation Study.  
395 *NeuroImage* 59 (4), 4141–59.  
396 URL <http://dx.doi.org/10.1016/j.neuroimage.2011.10.010>
- 397 Allen, P. J., Polizzi, G., Krakow, K., Fish, D. R., Lemieux, L., 1998. Identification of EEG Events in  
398 the MR Scanner: the Problem of Pulse Artifact and a Method for Its Subtraction. *NeuroImage*  
399 8 (3), 229–239.
- 400 Calhoun, V. D., Adali, T., 2012. Multisubject Independent Component Analysis of fMRI: a Decade of  
401 Intrinsic Networks, Default Mode, and Neurodiagnostic Discovery. *Biomedical Engineering, IEEE*  
402 *Reviews in* 5, 60–73.
- 403 Calhoun, V. D., Adali, T., Pearlson, G. D., Pekar, J. J., 2001. A Method for Making Group Inferences  
404 From Functional MRI Data Using Independent Component Analysis. *Human Brain Mapping* 14 (3),  
405 140–51.  
406 URL <http://www.ncbi.nlm.nih.gov/pubmed/11559959>
- 407 Calhoun, V. D., de Lacy, N., 2017. Ten key observations on the analysis of resting-state functional mr  
408 imaging data using independent component analysis. *Neuroimaging Clinics* 27 (4), 561–579.
- 409 Calhoun, V. D., Kiehl, K. A., Pearlson, G. D., 2008. Modulation of Temporally Coherent Brain  
410 Networks Estimated Using ICA at Rest and During Cognitive Tasks. *Human Brain Mapping* 29 (7),  
411 828–838.
- 412 Calhoun, V. D., Miller, R., Pearlson, G., Adali, T., 2014. The Chronnectome: Time-Varying  
413 Connectivity Networks As the Next Frontier in fMRI Data Discovery. *Neuron* 84 (2), 262–274.
- 414 Chang, C., Glover, G. H., 2010. Time-Frequency Dynamics of Resting-State Brain Connectivity  
415 Measured With fMRI. *NeuroImage* 50 (1), 81–98.  
416 URL <http://www.pubmedcentral.nih.gov/articlerender.fcgi?artid=2827259&tool=pmcentrez&rendertype=abstract>
- 417
- 418 Choe, A. S., Nebel, M. B., Barber, A. D., Cohen, J. R., Xu, Y., Pekar, J. J., Caffo, B., Lindquist, M. A.,  
419 2017. Comparing test-retest reliability of dynamic functional connectivity methods. *NeuroImage*.
- 420 Cribben, I., Wager, T., Lindquist, M., 2013. Detecting functional connectivity change points for  
421 single-subject fMRI data. *Frontiers in computational neuroscience* 7, 143.
- 422 Damaraju, E., Allen, E. A., Belger, A., Ford, J. M., McEwen, S., Mathalon, D. H., Mueller, B. A.,  
423 Pearlson, G. D., Potkin, S. G., Preda, A., 2014. Dynamic Functional Connectivity Analysis Reveals  
424 Transient States of Dysconnectivity in Schizophrenia. *NeuroImage: Clinical* 5, 298–308.
- 425 Engle, R., 2002. Dynamic conditional correlation: A simple class of multivariate generalized autore-  
426 gressive conditional heteroskedasticity models. *Journal of Business & Economic Statistics* 20 (3),  
427 339–350.
- 428 Erhardt, E. B., Rachakonda, S., Bedrick, E. J., Allen, E. A., Adali, T., Calhoun, V. D., 2011.  
429 Comparison of Multi-Subject ICA Methods for Analysis of fMRI Data. *Human Brain Mapping*  
430 32 (12), 2075–2095.  
431 URL <http://dx.doi.org/10.1002/hbm.21170>

- 432 Friedman, J., Hastie, T., Tibshirani, R., 2008. Sparse Inverse Covariance Estimation With the  
433 Graphical Lasso. *Biostatistics* 9 (3), 432–441.  
434 URL <http://biostatistics.oxfordjournals.org/content/9/3/432.abstract>
- 435 Goupil, L., Bekinschtein, T., 2012. Cognitive processing during the transition to sleep. *Archives  
436 italiennes de biologie* 150 (2/3), 140–154.
- 437 Haimovici, A., Tagliazucchi, E., Balenzuela, P., Laufs, H., 2017. On wakefulness fluctuations as a  
438 source of BOLD functional connectivity dynamics. *Scientific Reports* 7.
- 439 Himberg, J., Hyvärinen, A., Esposito, F., 2004. Validating the Independent Components of Neu-  
440 roimaging Time Series Via Clustering and Visualization. *NeuroImage* 22 (3), 1214–1222.
- 441 Hindriks, R., Adhikari, M. H., Murayama, Y., Ganzetti, M., Mantini, D., Logothetis, N. K., Deco, G.,  
442 2016. Can sliding-window correlations reveal dynamic functional connectivity in resting-state fmri?  
443 *Neuroimage* 127, 242–256.
- 444 Hori, T., Hayashi, M., Morikawa, T., 1994. Topographical EEG changes and the hypnagogic experience.
- 445 Hutchison, R. M., Womelsdorf, T., Allen, E. A., Bandettini, P. A., Calhoun, V. D., Corbetta, M.,  
446 Penna, S. D., Duyn, J., Glover, G., Gonzalez-Castillo, J., 2013. Dynamic Functional Connectivity:  
447 Promises, Issues, and Interpretations. *NeuroImage*.
- 448 Jagannathan, S. R., Ezquerro-Nassar, A., Jachs, B., Pustovaya, O. V., Bareham, C. A., Bekinschtein,  
449 T. A., 2018. Tracking wakefulness as it fades: Micro-measures of alertness. *NeuroImage* 176, 138 –  
450 151.  
451 URL <http://www.sciencedirect.com/science/article/pii/S1053811918303562>
- 452 Kang, J., Wang, L., Yan, C., Wang, J., Liang, X., He, Y., 2011. Characterizing dynamic functional  
453 connectivity in the resting brain using variable parameter regression and kalman filtering approaches.  
454 *Neuroimage* 56 (3), 1222–1234.
- 455 Laumann, T. O., Snyder, A. Z., Mitra, A., Gordon, E. M., Gratton, C., Adeyemo, B., Gilmore,  
456 A. W., Nelson, S. M., Berg, J. J., Greene, D. J., McCarthy, J. E., Tagliazucchi, E., Laufs, H.,  
457 Schlaggar, B. L., Dosenbach, N. U. F., Petersen, S. E., 2016. On the Stability of BOLD fMRI  
458 Correlations. *Cerebral Cortex*.  
459 URL [http://cercor.oxfordjournals.org/content/early/2016/09/01/cercor.bhw265.  
460 abstract](http://cercor.oxfordjournals.org/content/early/2016/09/01/cercor.bhw265.abstract)
- 461 Leonardi, N., Van De Ville, D., 2015. On Spurious and Real Fluctuations of Dynamic Functional  
462 Connectivity During Rest. *NeuroImage* 104, 430–436.
- 463 Liegeois, R., Laumann, T. O., Snyder, A. Z., Zhou, J., Yeo, B. T., 2017. Interpreting temporal  
464 fluctuations in resting-state functional connectivity MRI. *Neuroimage*.
- 465 Lindquist, M. A., Xu, Y., Nebel, M. B., Caffo, B. S., 2014. Evaluating Dynamic Bivariate Correlations  
466 in Resting-State fMRI: a Comparison Study and a New Approach. *NeuroImage* 101, 531–46.  
467 URL <http://www.sciencedirect.com/science/article/pii/S1053811914005291>
- 468 Matsui, T., Murakami, T., Ohki, K., 2018. Neuronal origin of the temporal dynamics of spontaneous  
469 bold activity correlation. *Cerebral Cortex*.  
470 URL [+http://dx.doi.org/10.1093/cercor/bhy045](http://dx.doi.org/10.1093/cercor/bhy045)
- 471 Miller, R. L., Yaesoubi, M., Turner, J. A., Mathalon, D., Preda, A., Pearlson, G., Adali, T., Calhoun,  
472 V. D., 2016. Higher dimensional meta-state analysis reveals reduced resting fMRI connectivity  
473 dynamism in schizophrenia patients. *PloS one* 11 (3), e0149849.

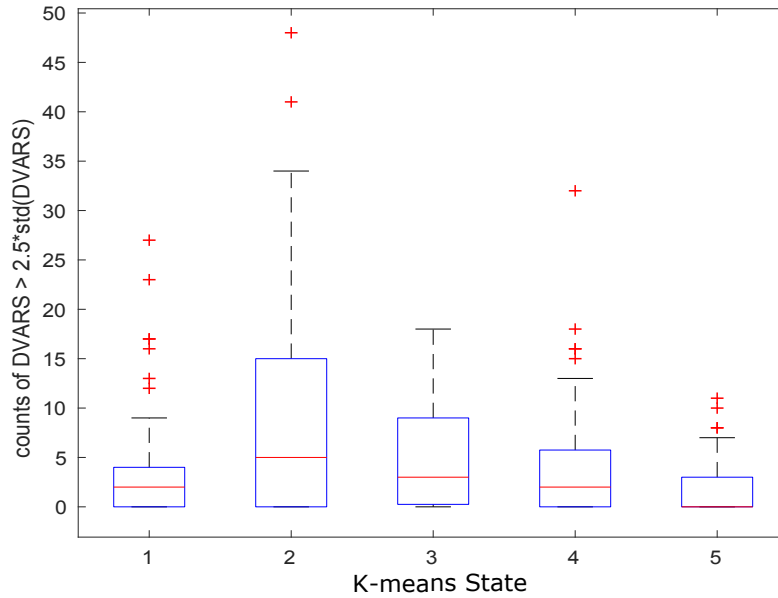
- 474 Power, J. D., Barnes, K. A., Snyder, A. Z., Schlaggar, B. L., Petersen, S. E., 2012. Spurious But  
475 Systematic Correlations in Functional Connectivity MRI Networks Arise From Subject Motion.  
476 *NeuroImage* 59 (3), 2142–54.  
477 URL <http://dx.doi.org/10.1016/j.neuroimage.2011.10.018>
- 478 Preti, M. G., Bolton, T. A., Van De Ville, D., 2017. The dynamic functional connectome: state-of-  
479 the-art and perspectives. *Neuroimage* 160, 41–54.
- 480 Rubinov, M., Sporns, O., 2011. Weight-Conserving Characterization of Complex Functional Brain  
481 Networks. *NeuroImage* 56 (4), 2068–2079.
- 482 Sakoğlu, U., Pearlson, G. D., Kiehl, K. A., Wang, Y. M., Michael, A. M., Calhoun, V. D., 2010. A  
483 method for evaluating dynamic functional network connectivity and task-modulation: Application  
484 to schizophrenia. *Magnetic Resonance Materials in Physics, Biology and Medicine* 23 (5-6), 351–366.
- 485 Shakil, S., Lee, C.-H., Keilholz, S. D., 2016. Evaluation of Sliding Window Correlation Performance  
486 for Characterizing Dynamic Functional Connectivity and Brain States. *NeuroImage* 133, 111–128.
- 487 Shine, J. M., Oluwasanmi, K., Bell, P. T., Gorgolewski, K. J., Gilat, M., Poldrack, R. A., 2015. Esti-  
488 mation of Dynamic Functional Connectivity Using Multiplicative Analytical Coupling. *NeuroImage*  
489 122, 399–407.  
490 URL <http://www.sciencedirect.com/science/article/pii/S1053811915006849>
- 491 Shirer, W. R., Ryali, S., Rykhlevskaia, E., Menon, V., Greicius, M. D., 2012. Decoding Subject-Driven  
492 Cognitive States With Whole-Brain Connectivity Patterns. *Cerebral Cortex* 22 (1), 158–165.
- 493 Smith, S. M., Fox, P. T., Miller, K. L., Glahn, D. C., Fox, P. M., Mackay, C. E., Filippini, N.,  
494 Watkins, K. E., Toro, R., Laird, A. R., Beckmann, C. F., 2009. Correspondence of the Brain’s  
495 Functional Architecture During Activation and Rest. *Proceedings of the National Academy of  
496 Sciences* 106 (31), 13040–5.  
497 URL <http://www.pnas.org/cgi/content/abstract/106/31/13040>
- 498 Smith, S. M., Miller, K. L., Salimi-Khorshidi, G., Webster, M., Beckmann, C. F., Nichols, T. E.,  
499 Ramsey, J. D., Woolrich, M. W., 2011. Network Modelling Methods for fMRI. *NeuroImage* 54 (2),  
500 875–891.
- 501 Tagliazucchi, E., Balenzuela, P., Fraiman, D., Chialvo, D. R., 2012a. Criticality in large-scale brain  
502 fMRI dynamics unveiled by a novel point process analysis. *Frontiers in physiology* 3, 15.
- 503 Tagliazucchi, E., von Wegner, F., Morzelewski, A., Borisov, S., Jahnke, K., Laufs, H., 2012b. Automatic  
504 sleep staging using fMRI functional connectivity data. *NeuroImage* 63 (1), 63 – 72.  
505 URL <http://www.sciencedirect.com/science/article/pii/S1053811912006507>
- 506 van der Maaten, Laurens, Hinton, Geoffrey, 2008. Visualizing data using t-SNE. *The Journal of  
507 Machine Learning Research* 9 (2579-2605), 85.
- 508 Vergara, V., Calhoun, V. D., 2018. Which dFNC Window Length is Valid? In: *Organization of  
509 Human Brain Mapping*. Singapore.
- 510 Vidaurre, D., Smith, S. M., Woolrich, M. W., 2017. Brain network dynamics are hierarchically  
511 organized in time. *Proceedings of the National Academy of Sciences* 114 (48), 12827–12832.  
512 URL <http://www.pnas.org/content/114/48/12827>
- 513 Wang, C., Ong, J. L., Patanaik, A., Zhou, J., Chee, M. W., 2016. Spontaneous eyelid closures link  
514 vigilance fluctuation with fMRI dynamic connectivity states. *Proceedings of the National Academy  
515 of Sciences* 113 (34), 9653–9658.

- 516 Yaesoubi, M., Allen, E. A., Miller, R. L., Calhoun, V. D., 2015a. Dynamic coherence analysis of  
517 resting fMRI data to jointly capture state-based phase, frequency, and time-domain information.  
518 *NeuroImage* 120, 133 – 142.  
519 URL <http://www.sciencedirect.com/science/article/pii/S1053811915006096>
- 520 Yaesoubi, M., Miller, R. L., Calhoun, V. D., 2015b. Mutually temporally independent connectivity  
521 patterns: A new framework to study the dynamics of brain connectivity at rest with application to  
522 explain group difference based on gender. *NeuroImage* 107, 85–94.
- 523 Yu, Q., Du, Y., Chen, J., He, H., Sui, J., Pearlson, G., Calhoun, V. D., 2017. Comparing brain graphs  
524 in which nodes are regions of interest or independent components: A simulation study. *Journal of*  
525 *neuroscience methods* 291, 61–68.
- 526 Zalesky, A., Breakspear, M., 2015. Towards a statistical test for functional connectivity dynamics.  
527 *NeuroImage* 114, 466 – 470.  
528 URL <http://www.sciencedirect.com/science/article/pii/S1053811915002293>



## 5. Supplementary data

**A**



**B**

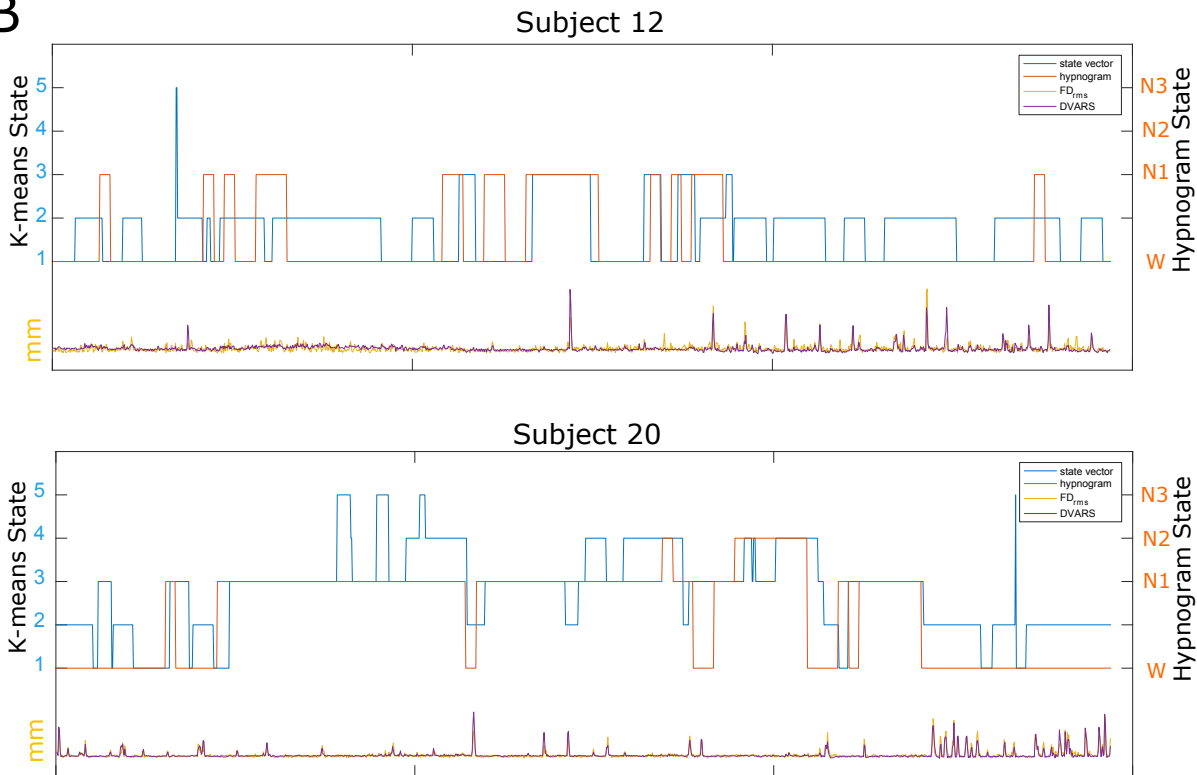


Figure S1: A) Count of number of DVARS of raw data exceeding 2.5 times its standard deviation by K-means state assignment. One-way ANOVA on mean differences in counts is significant with  $F=8.9$  and  $p < 1e-05$ . A similar result is observed using subject FD values. B) Example subject state vector plotted along with his/her hypnogram and head movement summaries (DVARS and FD). As seen, State 2 FC estimates seems to be contaminated by bigger jerky movements from subjects. .

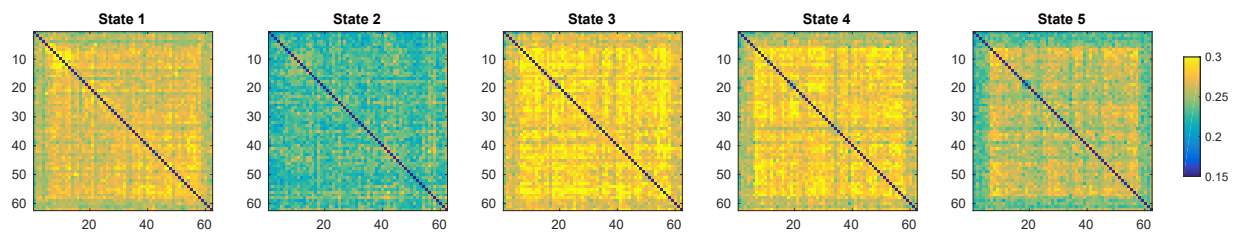


Figure S2: Standard deviation of the dFNC estimates by K-means state. The standard deviation increases for most pairs for States 3 and 4 compared wakeful state 1 and the variability of dFC reduces during deep sleep stage N3.